

Research Article

Optimization of Wall Materials for Astaxanthin Powder Production from Shrimp Shell Extract Using Simplex Lattice Mixture Design

P. Sharayei ¹, E. Azarpazhooh ¹, S. Einafshar ¹, Sh. Zomorodi ², F. Zare ³,
and Hosahalli S. Ramaswamy ⁴

¹Agricultural Engineering Research Department, Khorasan Razavi Agricultural and Natural Resources Research and Education Center, AREEO, Mashhad, Iran

²Agricultural Engineering Research Department, West Azerbaijan Agricultural and Natural Resources Research and Education Center, AREEO, Urmia, Iran

³Northern Crops Institute, North Dakota State University, Fargo, North Dakota, USA

⁴Department of Food Science and Agricultural Chemistry, Macdonald Campus of McGill University, 2111 Lakeshore Road, Ste. Anne de Bellevue, Quebec, Canada H9X 3V9

Correspondence should be addressed to P. Sharayei; parvin_sharayei@yahoo.com

Received 5 September 2023; Revised 25 February 2024; Accepted 27 February 2024; Published 21 March 2024

Academic Editor: Sanju Bala Dhull

Copyright © 2024 P. Sharayei et al. This is an open access article distributed under the Creative Commons Attribution License, which permits unrestricted use, distribution, and reproduction in any medium, provided the original work is properly cited.

Shrimp shell waste is an attractive source of value-added bioactive-rich by-products. Shrimp shell extract containing astaxanthin was recovered by solvent extraction method (petroleum ether/acetone/water with a ratio of 15:75:10) and ultrasound process (amplitude 20% for 15 min at 35°C). The extract was then encapsulated by freeze-drying using wall materials such as maltodextrin (with the dextrose equivalent (DE) of 7 (MD7) and 20 (MD20)) and modified starch (Hi-Cap 100) incorporated at different ratios. Simplex lattice with augmented axial points in the mixture design was applied for the optimization of wall material. The optimal wall materials were 29.4% (MD7), 34.0% (Hi-Cap 100), and 36.6% (MD20), with encapsulation yield (Y) of 94.6%, encapsulation efficiency (EE) of 91.8%, astaxanthin content (Ast) of 46.1 µg/g DW, and DPPH scavenging capacity of 64.0%, respectively. The optimized microcapsules had spongy morphology and brittle and flaky mass. The degradation kinetics of bioactive astaxanthin in UV light was evaluated and found to follow first-order reaction kinetics. The microcapsules obtained under optimal wall composition exhibited the highest UV light stability with half-life values of 76.8 h, demonstrating a high stability.

1. Introduction

Food, pharmaceutical, and health items all employ food color additives widely. Food industry was forced to develop functional food items using natural pigments like carotenoids due to rising consumer awareness of and governmental actions against synthetic colorants [1]. Astaxanthin is a carotenoid pigment that is well-known for its reddish-orange color and a variety of health benefits. It improves biological processes, including lowering the oxidation of fatty acids, enhancing vitamin A production, stimulating growth, and potentially preventing diseases such as high

cholesterol, Alzheimer's, and Parkinson's. It has been used as a feed additive in aquaculture and poultry farming to enhance the coloration of the flesh of farm-raised aquatic animals and eggs of birds [2, 3]. Therefore, the global astaxanthin market was valued at USD 647.1 million in 2021, and it is expected to grow at a compound annual growth rate (CAGR) of 9.7% until 2026 (<https://www.grandviewresearch.com/industry-analysis/global-astaxanthin-market>) [4].

The use of natural astaxanthin is limited by its low stability, weak tinctorial strength, inability to match the desired hue, and probable interactions with other food ingredients [5]. Encapsulation has been extensively studied as a technology

to enhance astaxanthin stability. The correct choice of the wall material and drying method has affected the encapsulation efficiency and stability of the microcapsules [6].

Although, various astaxanthin encapsulation methods [7–11] with different coating or wall materials [12–15] have been reported; limited information are available on the astaxanthin microencapsulation with maltodextrin or modified starch by freeze-drying method.

Maltodextrin (with different dextrose equivalent) is a partially hydrolyzed product of starch that can be used to encapsulate bioactive compounds [16, 17]. Hi-Cap 100 starch, also known as modified starch or starch octenyl succinate, is commonly produced by esterification of starch with octenylsuccinic anhydride in aqueous media under alkaline conditions. This process adds hydrophobic side chains to the hydrophilic starch molecules, giving them amphiphilic properties. As a result, in two-phase water-oil systems, the hydrophobic side chains of the starch adhere to the surfaces of oil droplets; in contrast, the hydrophilic side chains interact with water molecules, creating steric repulsion and preventing droplet coalescence [18].

The coating materials and drying methods have a significant impact on the antioxidant activity, constancy, solvability, and retention of the encapsulated bioactive compounds. Microencapsulation of astaxanthin has been achieved through spray-drying or freeze-drying methods [13]. The practical multistep freeze-drying approach is often used to dry and encapsulate unstable and heat-sensitive compounds [19].

Despite the extensive efforts in encapsulating astaxanthin, the encapsulation of astaxanthin extracted from shrimp shell waste, which is a valuable and abundant source of astaxanthin, using the freeze-drying technique and wall components such as maltodextrin and modified starch, has not been investigated.

The objective of this study was to develop encapsulated shrimp shell extract containing astaxanthin using modified starch (Hi-Cap 100) and maltodextrin with varying dextrose equivalent values (DE 7 and 20) through freeze-drying. Optimization was carried out utilizing a simplex lattice mixture design (due to simplicity, efficiency, and the ability to explore a wide range of factors). Additionally, the study assessed the UV light stability of the microcapsules during storage.

2. Materials and Methods

2.1. Chemicals and Reagents. Analytical grade solvents, 2,2-diphenyl-1-picrylhydrazyl (DPPH) radicals, 2,4,6-Tri(2-pyridyl)-s-triazine (TPTZ), the Folin-Ciocalteu reagent, and maltodextrin with dextrose equivalents of 7 and 20 (MD7 and MD20) were obtained from Sigma-Aldrich and Merck companies. Hi-Cap 100 (modified starch with octenyl succinate substituents of 5% moisture and more than 90% solubility in water) was provided from the National Starch Company of the U.K.

2.2. Preparation of Freeze-Dried Shrimp Shell Extract. Green tiger shrimp shells were used to extract astaxanthin using a

solvent-assisted ultrasonic process [20]. For carrying out extraction, a 10 g sample of milled shrimp shell was placed in the 100 mL flask, to which 40 mL of solvent (petroleum ether: acetone: water, 15:75:10) was added (1:4 w/v), and the mixture was subjected to ultrasound waves (Hielscher, Germany Ultrasonic Electronic Equipment Co. Ltd., with a maximum power of 400 W and a frequency of 20 kHz) for 15 minutes at a temperature of 35°C and an amplitude of 20%. Following the sonication, the mixture was transferred to a Soxhlet device for solvent extraction of 6 h. When the extraction process was completed, the mixture was filtered, and the solvent was concentrated in a vacuum rotary evaporator (Laborota 4000 efficient, Germany). Then, the concentrate was dried in a freeze drier (Operon-Korea) (−55°C, 0.15 mmHg) for 48 h and kept in the dark at −18°C for further analysis. The amount of astaxanthin, ferric reducing antioxidant power, and free radical scavenging capacity of the freeze-dried shrimp shell extract was 51.5 µg/g, 1705 µmol of Fe²⁺/g, and 73.9%, respectively [20].

2.3. Preparation of Microencapsulated Powders. Different amounts of MD7, MD20, and Hi-Cap 100 were dissolved in distilled water at ambient temperature (25 ± 1°C) to achieve a total solid concentration of 10%, following a response surface methodology (RSM) design (Table 1). The solutions were agitated for 30 minutes and then refrigerated at 4 ± 1°C for 24 h to complete the hydration process. The freeze-dried shrimp shell extract was added to the solutions at proportion 1:5 (W/W, shrimp shell extract: wall materials) and homogenized by an Ultra-Turrax homogenizer (T50, IKA company of Germany) at 15,000 rpm for 10 min. Subsequently, solutions containing coating and core materials were sonicated (Hielscher, Germany Ultrasonic Electronic Equipment Co. Ltd., 400 W, 20 KHz, diameter probe: 13 mm) for 3 min at room temperature. Finally, the solutions were dried in a freeze-dryer at −55°C for 48 h at a pressure of 0.15 mmHg. The dried specimens were ground (using a pestle and mortar) and passed a 0.71 mm mesh and stored in brown glass at −18°C for further analysis [21].

2.4. Determination of the Physical Properties of Microcapsules. The moisture content of encapsulated powders was determined using an infrared moisture analyzer (MX-50, Japan) at 105 ± 1°C [22].

The encapsulation yield (*Y*) was calculated based on dry matter measurements using the following formula (Eq. (1)), as described by Fang and Bhandari [23].

$$Y = \frac{\text{Microencapsulated powder (g)}}{\text{Core (g) + wall materials (g)}} \times 100. \quad (1)$$

The bulk density (g/cm³) of encapsulated powders was measured according to the method described by Tonon et al. [24].

The particle size of the microencapsulated powders, in terms of diameter, was determined using a laser diffraction particle size analyzer (SALD-2101, Shimadzu, Kyoto, Japan) based on the procedure by Parrarud and Pranee [25].

TABLE 1: Experimental design and mass fraction of three wall components according to simplex lattice mixture design.

Mixtures	Wall proportions (uncoded values)		
	MD7	Hi-Cap 100	MD20
1	0	50	50
2	50	0	50
3	0	0	100
4	50	50	0
5	100	0	0
6	16.67	66.67	16.67
7	100	0	0
8	0	100	0
9	0	0	100
10	16.67	16.67	66.67
11	66.67	16.67	16.67
12	33.33	33.33	33.33
13	50	50	0
14	0	100	0

The determination of the glass transition temperature (T_g) was carried out using a differential scanning calorimeter (DSC) instrument (DSC1 Mettler Toledo, Switzerland) according to the method described by Mahalleh et al. [26].

2.5. Determination of the Chemical Properties and Antioxidative Activity of Microcapsules. The encapsulation efficiency of microencapsulated powder was calculated according to the method described by Montero et al. [27] and in

$$EE = \frac{T_{Ast} - S_{Ast}}{T_{Ast}} \times 100, \quad (2)$$

where T_{Ast} and S_{Ast} are the total and surface astaxanthin content of the freeze-dried microcapsules.

The total astaxanthin content of microcapsules was determined as follows: 100 mg of the powder was thoroughly mixed with a mixture of ethanol, acetic acid, and water (with a 42:8:50 ratio) with a magnetic stirrer for 2 min. Then, 5 ml of hexane was added, stirred, and centrifuged at 5000 g for 5 min at 25°C. The absorbance of the supernatant hexane phase was measured according to the method described by Sachindra and Mahendrakar [28].

$$AST \left(\frac{\mu g}{g} \right) = \frac{A \times D \times 10^6}{100 \times G \times d \times E_{1cm}^{1\%}}, \quad (3)$$

where Ast is the astaxanthin concentration in $\mu g/g$, A is the absorbance at 470 nm, D is the extract volume in hexane, 10^6 is the dilution multiple, G is the sample weight in g, d is the cuvette width, and E is the extinction coefficient, 2100 [28].

The amount of surface astaxanthin was determined by washing 100 mg of the microencapsulated powder twice with 2 mL of hexane. Each washing step lasted 5 s. After an appropriate dilution, the absorbance of hexane was measured, and the amount of surface astaxanthin was determined using Eq. (3).

Free radical scavenging activity was evaluated by 2,2-diphenyl-1-picrylhydrazyl (DPPH) assay according to Ramadan et al.'s [29] method using

$$DPPH\% = \left[\frac{A_{DPPH} - A_S}{A_{DPPH}} \right] \times 100, \quad (4)$$

where A_S is the DPPH solution absorbance when the extract has been added at a specified amount and A_{DPPH} is the DPPH solution absorbance.

2.6. Scanning Electron Microscopy. Scanning electron microscopy was employed to examine the particle structures of the prepared microcapsules. The analysis was conducted using a scanning electron microscope (LEO 1450, VP, Germany) following the method described by Ahmed et al. [30].

2.7. Evaluation of Stability of Encapsulated Powders to UV Light. The prepared microcapsules were packaged in low-density polyethylene plastic bags and subjected to UV light (four 15 W lamps, 254 nm, placed 20 cm away from the samples) for 10 h. Sampling was conducted initially (zero time) and every 2 h, and the amount of astaxanthin in the samples was measured.

The degradation kinetics of astaxanthin under UV light were determined by analyzing the rate constants with respect to time using Equation (5). Additionally, the half-life time ($T_{1/2}$) was calculated using Equations (6).

$$C_t = C_0 \exp(k \times t), \quad (5)$$

$$T_{1/2} = \frac{\ln(0.5)}{k} = \frac{0.693}{k}, \quad (6)$$

where C_0 is the initial astaxanthin content and C_t is the astaxanthin content after time t (min) while k is the first-order kinetic constant [31, 32].

2.8. Experimental Design and Statistical Analysis. In this study, a simplex lattice mixture design (a type of lattice design) based on the procedures outlined by Mahalleh et al. [26] was adopted to investigate the impact of MD7, MD20, and Hi-Cap 100 on the physicochemical characteristics of dried microencapsulated powder. The dependent variables (responses) were analyzed in relation to various physicochemical properties of the encapsulated powders. Multiple response optimizations were performed to identify the optimal combination of experimental factors that simultaneously optimize the responses. The component proportions were expressed as fractions of the mixture, with a sum of 100 ($A + B + C$). The levels of MD7, MD20, and Hi-Cap 100 and experimental design in terms of coded and uncoded values as 14 combinations are presented in Table 1. Design-Expert 11.0 software (Stat-Ease Inc., Minneapolis, USA) was utilized for regression analysis, as well as generating 3D surface and Cox response trace plots. The significance levels for statistical procedures were set at $P \leq 0.01$ and $P \leq 0.05$. Numerical optimization was used to find the best conditions for shrimp shell waste extract microencapsulation on responses. Experiments were aimed at maximizing

encapsulation yield, astaxanthin content, and antioxidant activity (free radical scavenging capacity). Means were compared using MstatC software. Analysis data on the stability kinetics of microcapsules were performed with ANOVA. ANOVA and regression analyses were performed using MstatC and Excel software. All measurements and trials were performed in triplicates, and significant differences between means were determined using multiple range tests by Duncan (P values less than 0.05 were considered statistically significant).

3. Results and Discussion

3.1. Model Fitting. Tables 2 and 3 summarize the results of using response surface methodology (RSM) to assess the impact of different wall materials (MD7, Hi-Cap 100, and MD20) on the physicochemical properties of shrimp shell extract encapsulation. In order to determine the experimental model for predicting the response, polynomial equations including linear, two factorial (interactive), quadratic, and cubic were fitted to the data obtained from the response surface methodology. These models were then statistically compared to determine the most optimal model for predicting the responses. The selected model should have a nonsignificant lack of fit and the highest values of R^2 and adjusted R^2 . The regression models in this study had R^2 and adjusted R^2 values greater than 0.70, indicating a good fit of the models to the data. Additionally, the Adeq precision values for all physicochemical parameters were higher than 4, which is desirable as it suggests a good signal-to-noise ratio.

To assess the accuracy of the proposed model, the experimental results were compared with the predicted values obtained from the mathematical models (Tables 2 and 3). The data were gathered around the predicted model, as seen by the plots of the predicted values against the experimental values; as a result, there is a positive correlation between the predicted and experimental values. Additionally, the residuals do not exhibit any particular pattern or structure, as shown by the plots of the residuals against the fitted values. Regression models are therefore suitable.

3.2. Physical Properties of the Microcapsules. Table 4 displays the average values for multiple responses, such as moisture, encapsulation yield, bulk density, particle size, and glass transition temperature.

The moisture content is a significant parameter that affects the efficiency of drying, powder flow, stickiness, and storage stability of the product [33, 34]. There was a significant difference in the moisture content of the microcapsules (7.9 to 12.5%) ($P < 0.05$). The equation to predict the moisture content response was derived using pseudocomponent values obtained from the mixture design (Eq. (7)). The equation is as follows, where A represents MD7, B represents Hi-Cap 100, and C represents MD20:

$$Y = 9.95A + 11.45B + 10.60C - 10.64AB - 1.93AC - 11.01BC - 8.56A^2BC - 69.40AB^2C + 222.11ABC^2. \quad (7)$$

The equation, expressed in coded factors, enables the prediction of the response at specific levels of each factor. In this coding system, the high levels of the mixture components are denoted as +1, while the low levels are represented as 0. This coded equation is useful for assessing the relative impact of each factor by comparing the coefficients associated with each factor.

Comparing the treatment means showed that higher concentrations of Hi-Cap 100 (100%) resulted in a significant rise in moisture content (12.5%, Table 4). The Cox response trace plot and response surface plot (Figures 1(a) and 1(b)) indicated that the moisture content of the microcapsules decreased as the levels of the wall materials approached the midpoint of the triangular design (where the three points have equal proportions). Overall, higher levels of MD7, Hi-Cap 100, and MD20 were associated with higher moisture content (Figures 1(a) and 1(b) and Table 4). This variability in moisture content might be attributed to the chemical structure and water affinity of the wall materials. Hydrocolloid materials with hydrophilic groups tend to bind water molecules, resulting in higher moisture retention [35]. Additionally, the use of maltodextrin as a coating wall has been reported to enhance drying speed due to its low resistance to mass transfer high solubility in water, low viscosity even at high solid content, neutral flavor, and colorless solutions, and they are readily available [36].

Based on Table 4, the encapsulation yield (Y) ranged from 85.2% to 95.5%. The analysis of variance revealed a statistically significant impact of the wall composition on the microencapsulation yield ($P < 0.05$). The relationship between the wall materials (MD7, Hi-Cap 100, and MD20) and Y was quadratic, and higher yields were obtained in microcapsules containing a mixture of MD7 (66.7% or 16.7%), Hi-Cap 100 (16.7%), and MD20 (16.7% or 66.7%). The regression equation for the Y response, expressed in terms of L -pseudocomponent values obtained from the mixture design, is presented in

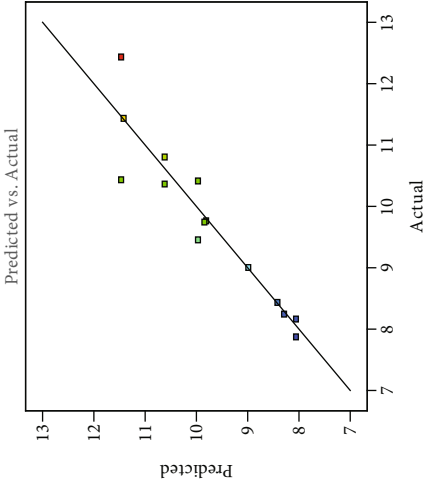
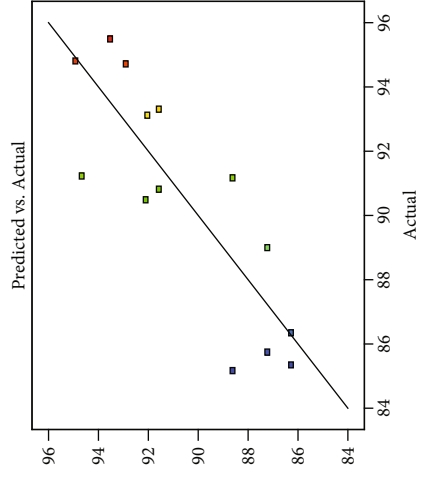
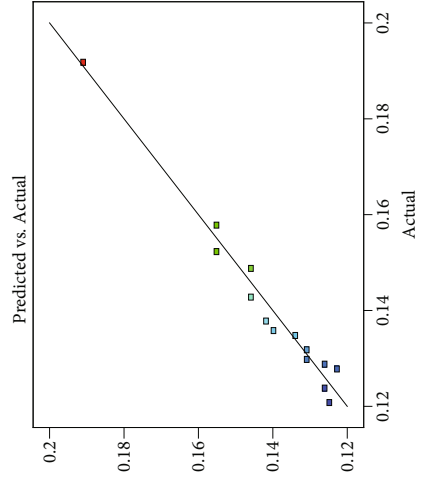
$$Y = 88.59A + 87.20B + 86.25C + 14.61AB + 29.89AC + 21.14BC. \quad (8)$$

The yield of encapsulation initially increased and then decreased upon increasing the amount of MD7 or MD20 up to 33.3% (where the three points have equal ratios) (Figures 1(c) and 1(d)). The plots also indicated that a lower value of Hi-Cap 100 leads to a higher encapsulation yield. The properties of the wall and core materials such as emulsification properties and drying parameters are those factors which affect the yield of encapsulating [37].

The bulk density of the microcapsules ranged from 0.121 to 0.192 g/cm³, and the interaction between the three components was found to be significant ($P < 0.05$). Among the microcapsules, those coated with Hi-Cap 100 and MD20 at a concentration of 50% exhibited the highest bulk density (0.192 g/cm³). The bulk density of powders can be influenced by factors like particle size, fragility, and fluidity. Moreover, the molecular weight of the wall materials also plays a role in determining the bulk density of the powders.

TABLE 2: ANOVA, predicted vs. actual, and residuals vs. predicted plots for physical parameters of microcapsules.

Fit statistics	Moisture (%)		Encapsulated yield (%)		Bulk density (mg/cc)	
	Quadratic ($P = <0.05$)	Quadratic ($P = <0.05$)	Quadratic ($P = <0.05$)	Quadratic ($P = <0.05$)	Special cubic ($P = <0.01$)	Special cubic ($P = <0.01$)
Lack of fit	$P = 0.90$	$P = 0.54$	$P = 0.061$			
R^2	0.89	0.84	0.97			
Adjusted R^2	0.71	0.71	0.93			
Adeq precision	5.89	5.24	17.31			

Predicted vs. actual plots	Moisture (%)		Encapsulated yield (%)		Bulk density (mg/cc)	
	Actual	Predicted	Actual	Predicted	Actual	Predicted
						

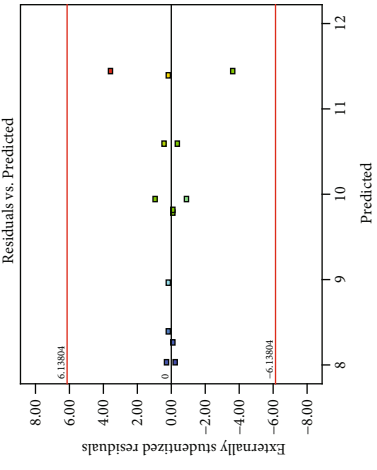
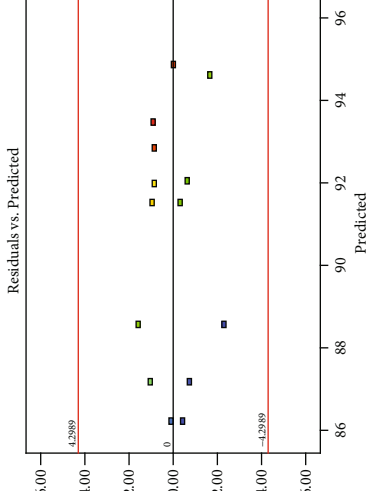
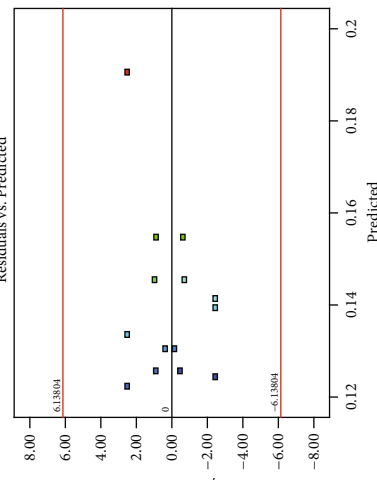
Residuals vs. predicted plots	Moisture (%)		Encapsulated yield (%)		Bulk density (mg/cc)	
	Predicted	Externally studentized residuals	Predicted	Externally studentized residuals	Predicted	Externally studentized residuals
						

TABLE 3: ANOVA, predicted vs. actual, and residuals plots for chemical parameters of microcapsules.

Fitted model	Encapsulation efficiency (%) Special cubic ($P = <0.01$)	Astaxanthin content ($\mu\text{g/g}$) Special cubic ($P = <0.01$)	DPPH radical scavenging power (%) Special cubic ($P = <0.01$)
Lack of fit	$P = 0.99$	$P = 0.97$	$P = 0.97$
R^2	0.92	0.88	0.87
Adjusted R^2	0.84	0.78	0.76
Adeq precision	11.12	9.58	8.84
Predicted vs. actual plots			
Residuals vs. predicted plots			

TABLE 4: The effect of type and concentration of wall compounds on physical properties of encapsulated powders.

MD7	Wall composition		Moisture (%)	Encapsulation yield (Y, %)	Bulk density (g/cm ³)	Particle size (μm)	Glass transition temperature (T _g , °C)
	Hi-Cap 100	MD20					
0	50	50	8.3 ± 0.51 g	93.2 ± 1.01b	0.192 ± 0.007a	34.1 ± 0.87b	51.4 ± 0.04e
50	0	50	9.8 ± 0.34de	94.8 ± 0.86b	0.135 ± 0.002de	—	—
0	0	100	10.4 ± 0.11cd	85.4 ± 2.18f	0.143 ± 0.003c	—	—
50	50	0	8.2 ± 0.90fg	93.3 ± 1.47b	0.124 ± 0.007gh	—	—
100	0	0	10.4 ± 0.64c	91.2 ± 1.11c	0.130 ± 0.003e	—	—
16.67	66.67	16.67	8.6 ± 0.76fg	90.5 ± 1.25cd	0.138 ± 0.001d	38.5 ± 1.25a	69.1 ± 0.01b
100	0	0	9.5 ± 0.77ef	85.2 ± 1.26f	0.132 ± 0.002e	—	—
0	100	0	12.5 ± 0.18a	89.0 ± 1.15d	0.158 ± 0.001b	—	—
0	0	100	10.8 ± 0.39c	86.4 ± 0.84ef	0.149 ± 0.004c	—	—
16.67	16.67	66.67	11.4 ± 0.16b	94.7 ± 1.7ab	0.136 ± 0.001d	31.6 ± 1.12c	68.9 ± 0.02b
66.67	16.67	16.67	9.0 ± 0.18e	95.5 ± 1.1a	0.121 ± 0.002h	31.9 ± 1.20c	64.2 ± 0.11c
33.33	33.33	33.33	9.8 ± 0.61de	91.3 ± 1.76c	0.128 ± 0.001fg	35.9 ± 0.94b	70.9 ± 0.08a
50	50	0	7.9 ± 0.03g	90.8 ± 0.45cd	0.129 ± 0.001f	35.1 ± 1.37b	57.6 ± 0.09d
0	100	0	11.4 ± 0.41bc	85.8 ± 0.58f	0.155 ± 0.001b	—	—

Means ± SD (standard deviation) within a column with the same lowercase letters are not significantly different at $P < 0.05$.

Smaller overall volume results in higher bulk density, as discussed by Mahdavi et al. [38].

Equation (9) represents the regression equation for bulk density response in terms of L -pseudocomponent values generated through mixture design.

$$Y = 0.131A + 0.155B + 0.146C - 0.068AB - 0.018AC + 0.162BC - 0.021A^2BC - 1.11AB^2C - 1.28ABC^2. \quad (9)$$

3.3. Particle Size, Glass Transition Temperature, and the Scanning Electron Microscopy. The average particle sizes (μm) of microcapsules obtained with various wall materials are shown in Table 4. The particle size of the microcapsules ranged from 31.9 to 38.5 μm. The composition of the wall material is the primary factor influencing the particle size of the microcapsules. The freeze-drying process can lead to a wide size range of microcapsules (20-5000 μm) due to the sublimation of ice crystals and longitudinal fractures, as observed by Azarpazhooh et al. [21]. Condurache et al. [39] reported size ranges of 8.5 to 81.2 μm and 31.2 to 43.5 μm for microencapsulated powders.

Table 4 presents a comparison of the glass transition temperature of the prepared microcapsules. The glass transition temperature is the temperature at which molecular movements begin in the polymer. The glass transition temperature of all microcapsules was higher than the ambient temperature. Moreover, microcapsules that contained the same amount of wall material exhibited higher glass transition temperatures than other microcapsules. Therefore, the softening of microcapsules were delayed at room temperature. The combination of MDs and Hi-Cap 100 may lead to increase stability and delay crystallinity in the microcapsules. The phenomenon of core material release and transfer through the wall material in the rubbery and soft state of the

polymer (temperature above the glass transition point) was reported by Chen et al. [40] and Azarpazhooh et al. [41].

According to the scanning electron microscope images (Figure 2), it is evident that the various types of prepared microcapsules lack a distinct geometric shape. This lack of uniformity may be attributed to the interplay of pressure and temperature during the freeze-drying process. The sublimation of ice crystals without a phase change leads to the retention of solid materials in a sponge-like, brittle, and flaky state. To safeguard the active compounds against heat and oxygen, glass structures are employed [42]. The formation of surface wrinkles and cavities on the surface of the microcapsule probably indicates the effect of mechanical stress and drying conditions on the wall materials. Mahalleh et al. [26] reported that the surface of freeze-dried microcapsules with Arabic gum and MD were brittle and dentate.

3.4. Chemical Properties of Microcapsules. Table 5 shows the encapsulation efficiency, astaxanthin content, and DPPH radical scavenging power. Encapsulation efficiency is the percentage of the active component that was successfully protected in the carrier material. Encapsulation efficiency was from 54.9 to 90.5%. Equation (10) represents the regression equation for EE response.

$$Y = 64.73A + 56.64B + 64.61C + 49.58AB + 20.23AC + 9078BC + 313.48ABC. \quad (10)$$

The encapsulating wall materials showed a significant effect on EE ($P < 0.05$). Several researches have revealed different astaxanthin encapsulation efficiency. Gomez-Estaca et al. [9] reported that the EE of the encapsulation of astaxanthin extracted from shrimp waste using complex coacervation with gelatin-cashew gum as core wall material followed by freeze-drying was 60%. Vakarelova et al. [43]

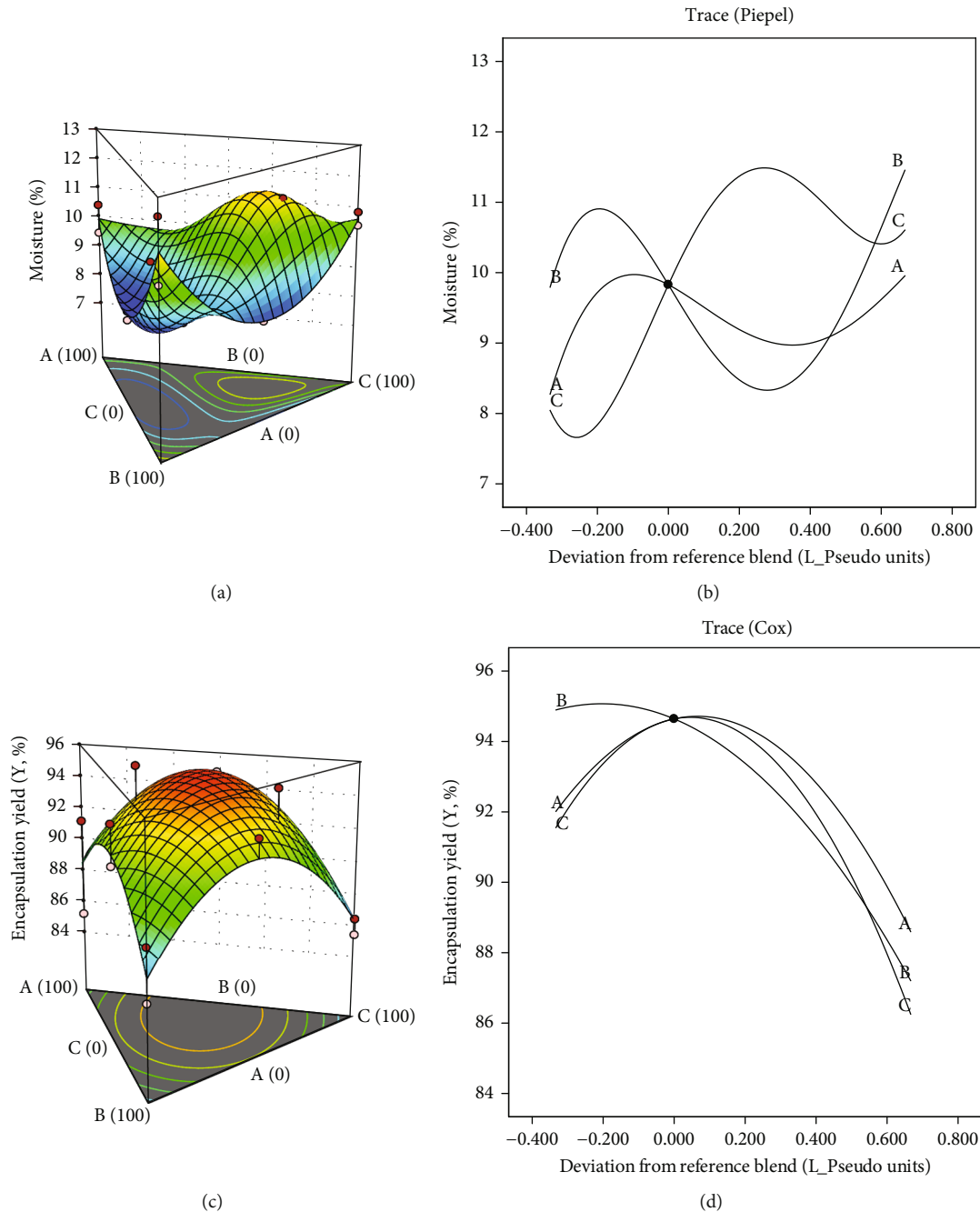


FIGURE 1: The effect of wall composition on the moisture content (%) and encapsulation yield (Y, %) of the microcapsules. (a, c) Response surface plots and (b, d) Cox plots. (A) MD7; (B) Hi-Cap 100; (C) MD20.

reported 62-65% EE via ionic gelation. Huang et al. [44] showed 85% EE via sodium caseinate and κ -carrageenan as wall materials. Other investigations have found EEs of 58.76% for carboxymethyl cellulose sodium (CMC-Na) [12], 94.34% for zein and oligochitosan [12], and various percents of EE for microcrystalline cellulose (MCC) [7].

Also, results showed that the combination of MD and Hi-Cap 100 in the wall material considerably enhanced EE ($P < 0.05$), indicating that using a single wall material is not sufficient to achieve the desired quality attributes of microencapsulation. Combining various components such

as carbohydrates, proteins, polysaccharides, and gums can lead to better results and help achieve maximum EE. As can be seen in Figures 2(a) and 2(b), EE increased by increasing wall level to the central point of the triangular design (33.3%) compared to the use of each coating individually ($P < 0.05$). The efficiency of encapsulation is influenced by various factors, including the properties of the coating and core materials, such as emulsifying properties and drying parameters [45].

The astaxanthin concentration of the microcapsules ranged from 28.8 to 45.1 $\mu\text{g/g}$ ($P < 0.05$) (Table 5). Equation

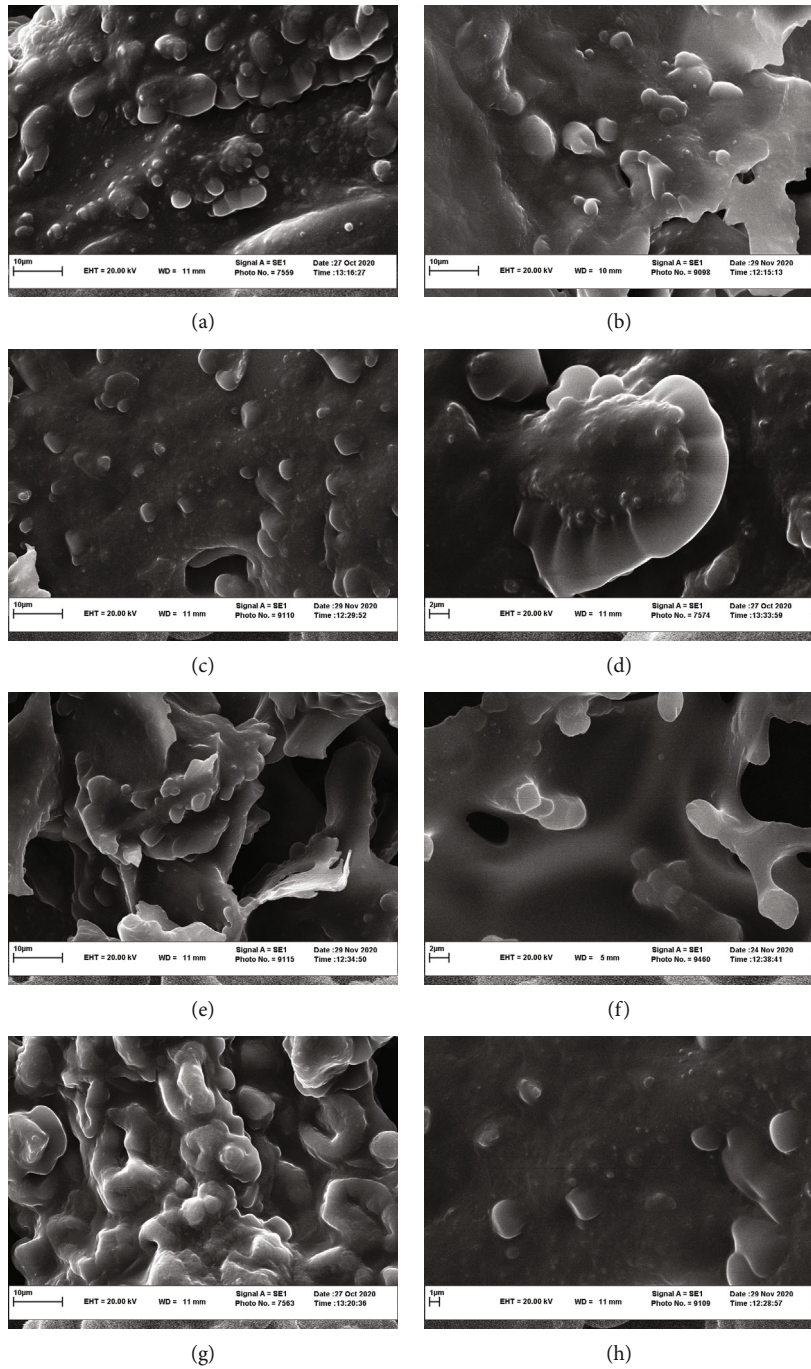


FIGURE 2: Continued.

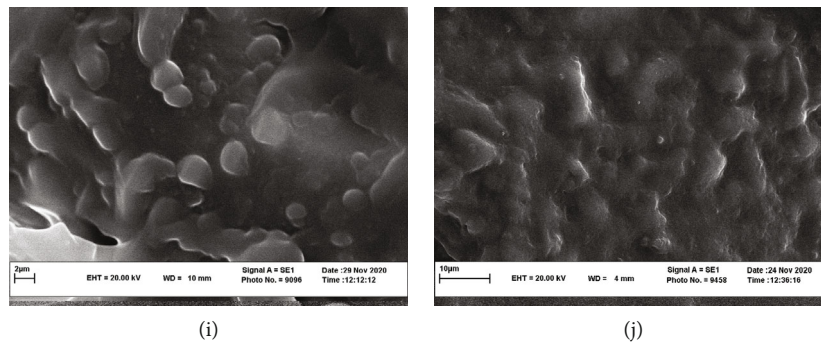


FIGURE 2: Scanning electron micrographs of freeze-dried encapsulated powders. (a) MD7 (50), Hi-Cap 100 (50), and MD20 (0); (b) MD7 (50), Hi-Cap 100 (0), and MD20 (50); (c) MD7 (0), Hi-Cap 100 (0), and MD20 (100); (d) MD7 (50), Hi-Cap 100 (50), and MD20 (0); (e) MD7 (100), Hi-Cap 100 (0), and MD20 (0); (f) MD7 (16.66), Hi-Cap 100 (66.67), and MD20 (16.66); (g) MD7 (100), Hi-Cap 100 (0), and MD20 (0); (h) MD7 (16.66), Hi-Cap 100 (16.66), and MD20 (66.67); (i) MD7 (66.67), Hi-Cap 100 (16.66), and MD20 (16.66); (j) MD7 (33.33), Hi-Cap 100 (33.33), and MD20 (33.33).

TABLE 5: The effect of type and concentration of wall compounds on chemical properties of encapsulated powders.

MD7	Wall composition		Encapsulation efficiency (EE, %)	Astaxanthin content (AST, $\mu\text{g/g}$)	DPPH radical scavenging power (DPPHsc, %)
	Hi-Cap 100	MD20			
0	50	50	$83.1 \pm 1.60\text{bc}$	$41.2 \pm 0.34\text{b}$	$55.6 \pm 0.75\text{c}$
50	0	50	$69.4 \pm 0.85\text{e}$	$35.2 \pm 0.73\text{e}$	$48.1 \pm 0.15\text{f}$
0	0	100	$59.9 \pm 0.23\text{f}$	$31.4 \pm 1.04\text{f}$	$40.9 \pm 0.42\text{h}$
50	50	0	$70.6 \pm 0.49\text{e}$	$35.8 \pm 0.56\text{e}$	$47.3 \pm 0.67\text{f}$
100	0	0	$58.6 \pm 1.35\text{f}$	$30.0 \pm 0.96\text{f}$	$42.2 \pm 1.07\text{g}$
16.67	66.67	16.67	$81.5 \pm 0.90\text{c}$	$41.3 \pm 0.76\text{bc}$	$56.44 \pm 0.57\text{c}$
100	0	0	$70.7 \pm 1.44\text{e}$	$36.9 \pm 0.14\text{g}$	$51.2 \pm 0.37\text{e}$
0	100	0	$58.5 \pm 0.79\text{f}$	$30.3 \pm 0.94\text{f}$	$40.5 \pm 0.25\text{h}$
0	0	100	$69.1 \pm 1.21\text{e}$	$35.5 \pm 0.41\text{e}$	$48.4 \pm 1.11\text{f}$
16.67	16.67	66.67	$83.9 \pm 0.98\text{b}$	$42.8 \pm 1.11\text{b}$	$58.9 \pm 0.21\text{b}$
66.67	16.67	16.67	$80.2 \pm 1.16\text{c}$	$40.8 \pm 0.96\text{cd}$	$54.9 \pm 0.24\text{d}$
33.33	33.33	33.33	$90.5 \pm 2.17\text{a}$	$45.1 \pm 0.76\text{a}$	$63.5 \pm 0.84\text{a}$
50	50	0	$75.5 \pm 1.30\text{d}$	$39.1 \pm 0.30\text{d}$	$51.8 \pm 1.37\text{e}$
0	100	0	$54.9 \pm 2.81\text{g}$	$28.8 \pm 0.94\text{f}$	$42.5 \pm 0.43\text{j}$

Means \pm SD (standard deviation) within a column with the same lowercase letters are not significantly different at $P < 0.05$.

(11) represents the regression equation correlating the response of astaxanthin content.

$$Y = 33.49A + 29.59B + 33.60C + 23.80AB + 7.78AC + 39.31BC + 157.89ABC \quad (11)$$

The quantity of astaxanthin in the Cox trace plot (Figure 3(d)) showed that the quantity of astaxanthin in the microcapsule increased significantly with increasing the coating concentration from 0 to 33.3% (the central point of the triangular simplex pattern) and then decreased by increasing coating concentration from 33.3 to 100%. This suggests that there is a coating concentration at which the astaxanthin content of the microcapsules can be maximized. Also, the results indicated that the higher equivalent of dextrose maltodextrin (DE) causes more astaxanthin protection in the capsule. The DE value of MD is in the range of 3–20,

indicating that it has a complex blend of high and low molecular weight compounds and a lengthy carbohydrate chain. The beneficial consequence of increasing the equivalence of dextrose is attributed to the decrease of the capsule's permeability to oxygen and thus the preservation of susceptible materials [46].

Table 5 shows the antioxidant capacity of the microcapsules ranged from 40.5 to 63.5%. Several studies have revealed the antioxidative properties of astaxanthin [47–49]. Astaxanthin has unique chemical properties due to its molecular structure, which plays an important role in scavenging free radicals and chelating heavy metals. The high antioxidant properties of astaxanthin are related to the presence of hydroxyl and keto fragments on the ionic ring. Astaxanthin inhibited free radicals both in the part of the unsaturated conjugated chain (polyani) and in the part of the terminal rings (c3 rings) [50].

Equation (12) represents the regression equation for DPPH radical scavenging power of astaxanthin in terms of

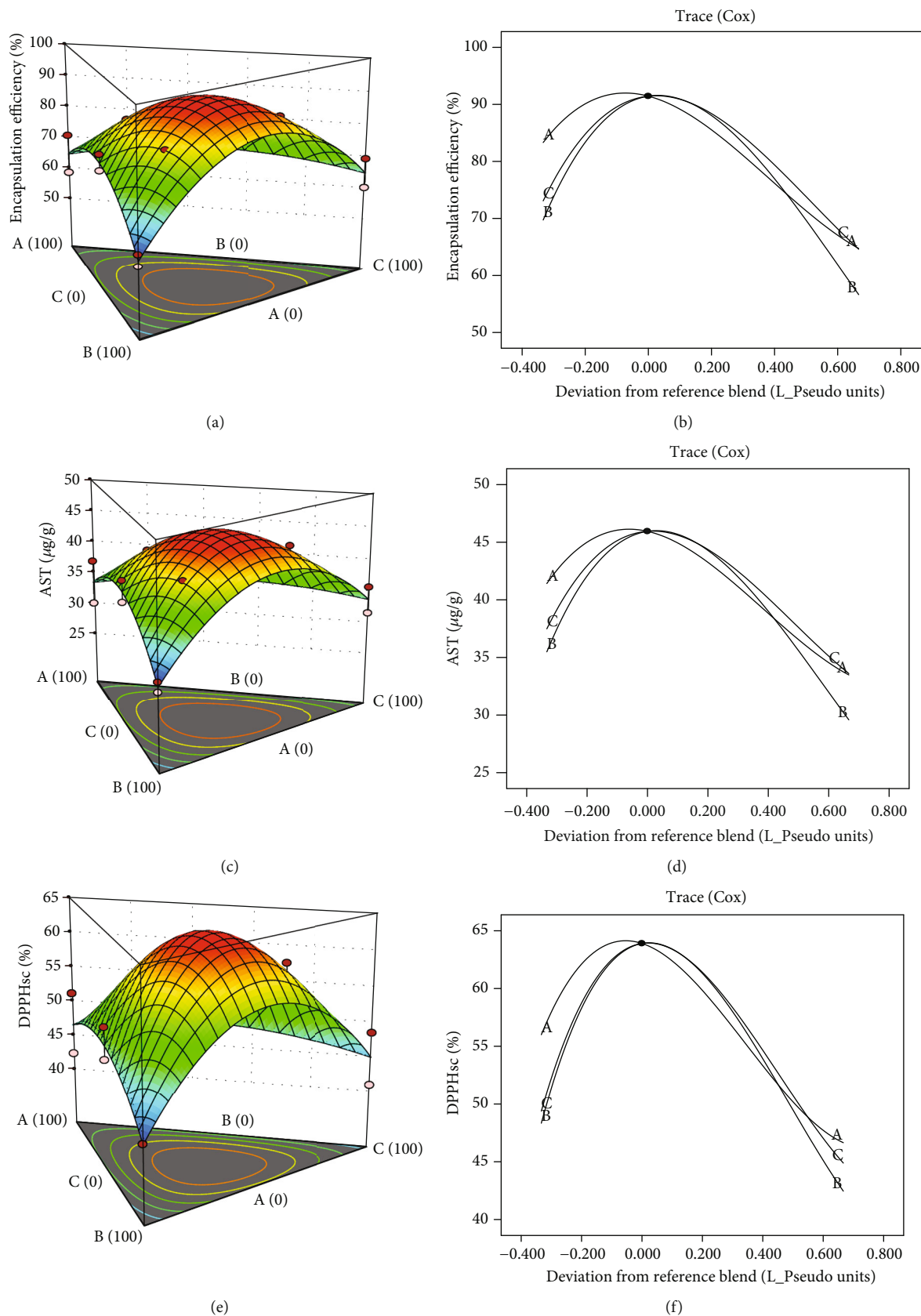


FIGURE 3: The effect of wall composition on the encapsulation efficiency (%), astaxanthin content (AST, $\mu\text{g/g}$), and DPPH radical scavenging power (DPPH_{sc}, %) of the microcapsules. (a, c, e) Response surface plots and (b, d, f) Cox plots. (A) MD7; (B) Hi-Cap 100; (C) MD20.

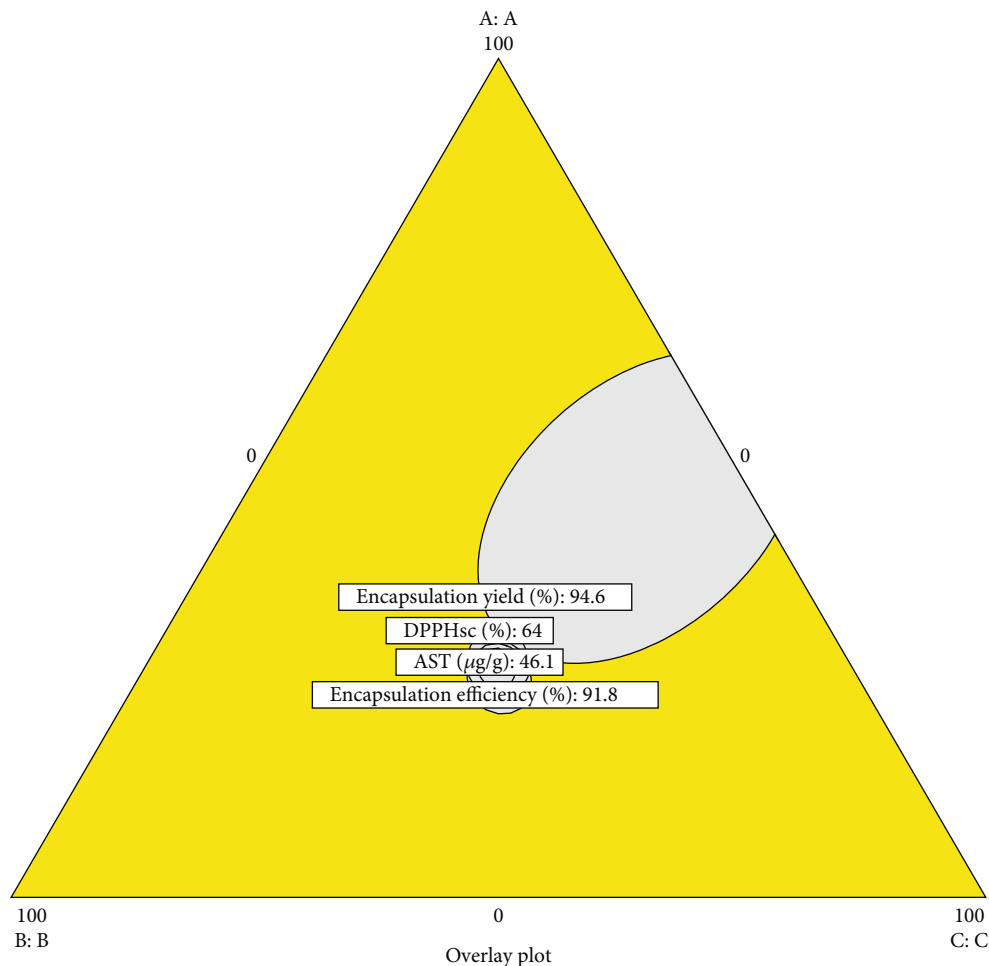


FIGURE 4: The overlay contour plot.

TABLE 6: Predicted and experimental values of the responses at optimum conditions.

	Encapsulation yield (%)	Encapsulation efficiency (%)	Astaxanthin content ($\mu\text{g/g}$)	DPPH radical scavenging power (%)
Predicted values ^a	94.6a*	91.8a	46.1a	64.0a
Experimental values ^b	93.9 \pm 0.97a	90.3 \pm 1.05a	47.1 \pm 0.72a	62.8 \pm 0.95a

Note: ^aPredicted using response surface quadratic model. ^bMean \pm standard deviation of triplicate determinations from experiments. *Data within a column with the same lowercase letters are not significantly different at $P < 0.05$.

L-pseudocomponent values generated through mixture design.

$$Y = 46.65A + 42.46B + 44.89C + 9.33AB + 10.29AC + 49.32BC + 282.61ABC. \quad (12)$$

Based on the findings of Cox and the response surface plots (Figures 3(e) and 3(f)), it was observed that the microcapsules formulated with MD20 exhibited more antioxidant activity at lower concentrations than those formulated with MD7. Additionally, the central point of the triangular design, which was encapsulated with MDs and Hi-Cap

100, was stronger than the wall material alone on preserving of the antioxidant components of the extract.

3.5. Optimization and Validation. The optimal conditions of the different wall material concentrations for the astaxanthin extract microencapsulation were determined using numerical optimization and graphical optimization of the software. The desired levels of each wall material include MD7, MD20, and Hi-Cap 100, while the dependent variables were optimized as maximum values. Dependent variables were analyzed individually. The Design-Expert software was employed to obtain the optimal conditions.

TABLE 7: The effect of UV light on the reaction rate constant, correlation coefficient, and half-life of astaxanthin in microcapsules.

MD7	Wall composition Hi-Cap 100	MD20	Reaction rate constant ($k \times 10^{-2}$) (h^{-1})	Half-life (h)	R^2	Retention astaxanthin (%)
0	50	50	0.036	19.4	0.97	69.9
50	0	50	0.045	15.3	0.99	63.4
0	0	100	0.0455	15.3	0.97	62.7
50	50	0	0.0445	15.6	0.99	64.4
100	0	0	0.0595	11.7	0.99	55.45
16.67	66.67	16.67	0.035	20.0	0.99	71.3
0	100	0	0.059	11.8	0.96	55.3
16.67	16.67	66.67	0.033	20.9	0.97	75.5
66.67	16.67	16.67	0.038	18.3	0.98	68.3
33.33	33.33	33.33	0.027	26.1	0.99	76.7
29.39	34.07	36.55	0.026	26.3	0.99	76.9
0	0	0	0.132	5.3	0.98	15.2

The optimal amounts of wall materials for microencapsulation were 29.4% (MD7), 34.0% (Hi-Cap 100), and 36.6% (MD20). The degree of desirability of the optimal point was 0.97. A degree of desirability above 0.8 can be considered to be suitable and/or acceptable. At the optimal type and concentration of wall materials, The encapsulation yield (Y), encapsulation efficiency (EE), astaxanthin content (Ast), and DPPH capacity were 94.6%, 91.8%, 46.1 $\mu\text{g/g}$, and 64.0%, respectively. The overlay graph is presented in Figure 4. Table 6 shows predicted and experimental values of the responses at optimum conditions. The models' efficiency was demonstrated by the lack of significant deviations between the models and the experimental observations ($P < 0.05$).

3.6. Stability of Encapsulated Powders to UV Light. Polar ionic rings and nonpolar conjugate bonds of astaxanthin absorb UV light and safeguard cells from oxidative damages [50]. The storage conditions influenced the astaxanthin retention rate. The more duration of light exposure caused the more astaxanthin release percentage. To better understand the decrease in astaxanthin levels under UV light irradiation, kinetic parameters such as the rate constant of astaxanthin reduction (K) and its half-life ($T_{1/2}$) were calculated (Table 7). The degradation of astaxanthin followed a first-order equation. Nonencapsulated astaxanthin was highly sensitive to UV light, leading to rapid degradation (with a higher reaction rate constant), so that only 15% of astaxanthin was retained after 10 hours of UV light exposure. Additionally, the astaxanthin reduction of microcapsules containing the equal percentage of MD7, MD20, and Hi-Cap 100 and optimal wall composition were lower than the others.

This finding is in accordance with that of Jiang and Zhu [12] who reported that after 9.5 hours of UV irradiation, the levels of astaxanthin in free and encapsulated forms were 60% and 82.4%, respectively.

4. Conclusions

In this research, freeze-dried shrimp shell extract was encapsulated by using maltodextrin (MD7 and MD20) and modi-

fied starch (Hi-Cap 100) as wall materials in a mass ratio of 1 : 5 (extract/wall material, w/w) and freeze-drying method. The resulting microcapsules exhibited particle sizes ranging from 31.9 to 38.5 μm , lacking a distinct geometric shape. A simplex lattice design with augmented axial points in a mixture design was used to optimize the wall materials. Under the optimized conditions, the highest encapsulation yield, encapsulation efficiency, astaxanthin content, and DPPH capacity were achieved, indicating the significance of the model employed. During a 10-hour UV light exposure, the investigation of astaxanthin compounds in the microencapsulated derived from shrimp shell waste extract demonstrated that the loss of astaxanthin was significantly influenced by the specific wall composition. Notably, the wall material with the same percentage of walls (33.3) and optimal wall composition (29.4% (MD7), 34.0% (Hi-Cap 100), and 36.6% (MD20)) exhibited remarkable stability, preserving the structural characteristics of the product and minimizing astaxanthin reduction compared to other wall materials.

Data Availability

The data of this article are taken from a research project that was carried out with the financial supports of INSF and the Agricultural Engineering Research Institute.

Additional Points

Practical Applications. This work fabricated a novel encapsulation system for astaxanthin extract from shrimp (green tiger) by-products through different wall materials and freeze-drying methodology. The optimized-microencapsulated astaxanthin powders showed proper physicochemical properties and were UV stable which make them possible to use in cosmetics, pharmaceuticals, food and beverage, and dietary supplements.

Conflicts of Interest

The authors declare that there is no conflict of interests.

Acknowledgments

The authors thank the Iran National Scientific Foundation (INSF) and Agricultural Engineering Research Institute (AERI) for the financial support (first author).

References

- [1] C. Lombardelli, I. Benucci, and M. Esti, "Novel food colorants from tomatoes: stability of carotenoid-containing chromoplasts under different storage conditions," *LWT-Food Science and Technology*, vol. 140, article 110725, 2021.
- [2] O. N. Kanwugu, A. R. Rao, G. A. Ravishankar, T. V. Glukharova, and E. G. Kovaleva, "Astaxanthin from bacteria as a feed supplement for animals," in *Global perspectives on Astaxanthin*, pp. 647–667, Academic press, 2021.
- [3] B. Li, J. Y. Lee, and Y. Luo, "Health benefits of astaxanthin and its encapsulation for improving bioavailability: a review," *Journal of Agriculture and Food Research*, vol. 14, p. 100685, 2023.
- [4] "Astaxanthin market by source (natural, synthetic), form (dry, liquid), method of production (microalgae cultivation, chemical synthesis, fermentation), application (dietary supplements, food and beverages, cosmetics), and region global forecast to 2026," 2023, <https://www.grandviewresearch.com/industry-analysis/global-astaxanthin-market>.
- [5] M. Cerreti, K. Liburdi, F. Del Franco, and M. Esti, "Heat and light stability of natural yellow colourants in model beverage systems," *Food Additives & Contaminants: Part A*, vol. 37, no. 6, pp. 905–915, 2020.
- [6] Ó. Martínez-Álvarez, M. M. Calvo, and J. Gómez-Estaca, "Recent advances in astaxanthin micro/nanoencapsulation to improve its stability and functionality as a food ingredient," *Marine Drugs*, vol. 18, no. 8, p. 406, 2020.
- [7] Z. Z. Feng, M. Y. Li, Y. T. Wang, and M. J. Zhu, "Astaxanthin from *Phaffia rhodozyma*: microencapsulation with carboxymethyl cellulose sodium and microcrystalline cellulose and effects of microencapsulated astaxanthin on yogurt properties," *LWT-Food Science and Technology*, vol. 96, pp. 152–160, 2018.
- [8] J. Gomez-Estaca, T. A. Comunian, P. Montero, and C. S. Fávoro-Trindade, "Physico-chemical properties, stability, and potential food applications of shrimp lipid extract encapsulated by complex coacervation," *Food and Bioprocess Technology*, vol. 11, no. 8, pp. 1596–1604, 2018.
- [9] J. Gomez-Estaca, T. A. Comunian, P. Montero, R. Ferro-Furtado, and C. S. Fávoro-Trindade, "Encapsulation of an astaxanthin-containing lipid extract from shrimp waste by complex coacervation using a novel gelatin–cashew gum complex," *Food Hydrocolloids*, vol. 61, pp. 155–162, 2016.
- [10] M. C. Gómez-Guillén, P. Montero, M. E. López-Caballero, G. C. Baccan, and J. Gómez-Estaca, "Bioactive and technological functionality of a lipid extract from shrimp (*L. vannamei*) cephalothorax," *LWT-Food Science and Technology*, vol. 89, pp. 704–711, 2018.
- [11] M. Qiang, X. Pang, D. Ma, C. Ma, and F. Liu, "Effect of membrane surface modification using chitosan hydrochloride and lactoferrin on the properties of astaxanthin-loaded liposomes," *Molecules*, vol. 25, no. 3, p. 610, 2020.
- [12] G. L. Jiang and M. J. Zhu, "Preparation of astaxanthin-encapsulated complex with zein and oligochitosan and its application in food processing," *LWT-Food Science and Technology*, vol. 106, pp. 179–185, 2019.
- [13] N. Khalid and C. J. Barrow, "Critical review of encapsulation methods for stabilization and delivery of astaxanthin," *Journal of Food Bioactives*, vol. 1, pp. 104–115, 2018.
- [14] C. Soukoulis and T. Bohn, "A comprehensive overview on the micro- and nano-technological encapsulation advances for enhancing the chemical stability and bioavailability of carotenoids," *Critical Reviews in Food Science and Nutrition*, vol. 58, no. 1, pp. 1–36, 2018.
- [15] D. F. Tirado, I. Palazzo, M. Scognamiglio, L. Calvo, G. Della Porta, and E. Reverchon, "Astaxanthin encapsulation in ethyl cellulose carriers by continuous supercritical emulsions extraction: a study on particle size, encapsulation efficiency, release profile and antioxidant activity," *The Journal of Supercritical Fluids*, vol. 150, pp. 128–136, 2019.
- [16] C. C. Loi, G. T. Eyres, P. Silcock, and E. J. Birch, "Application of a novel instantized glycerol monooleate ingredient in a protein-stabilized oil-in-water emulsion," *Food*, vol. 9, no. 9, p. 1237, 2020.
- [17] Z. Xiao, J. Xia, Q. Zhao, Y. Niu, and D. Zhao, "Maltodextrin as wall material for microcapsules: a review," *Carbohydrate Polymers*, vol. 298, article 120113, 2022.
- [18] S. Gupta, S. Khan, M. Muzafar, M. Kushwaha, A. K. Yadav, and A. P. Gupta, "Encapsulation: entrapping essential oil/flavors/aromas in food," in *Encapsulations*, A. M. Grumezescu, Ed., pp. 229–268, Academic Press, London, 2016.
- [19] T. A. Comunian, M. P. Silva, I. C. F. Moraes, and C. S. Fávoro-Trindade, "Reducing carotenoid loss during storage by co-encapsulation of pequi and buriti oils in oil-in-water emulsions followed by freeze-drying: use of heated and unheated whey protein isolates as emulsifiers," *Food Research International*, vol. 130, article 108901, 2020.
- [20] P. Sharayei, E. Azarpazhooh, S. Zomorodi, S. Einafshar, and H. S. Ramaswamy, "Optimization of ultrasonic-assisted extraction of astaxanthin from green tiger (*Penaeus semisulcatus*) shrimp shell," *Ultrasonics Sonochemistry*, vol. 76, p. 105666, 2021.
- [21] E. Azarpazhooh, P. Sharayei, S. Zomorodi, and H. S. Ramaswamy, "Physicochemical and phytochemical characterization and storage stability of freeze-dried encapsulated pomegranate peel anthocyanin and in vitro evaluation of its antioxidant activity," *Food and Bioprocess Technology*, vol. 12, no. 2, pp. 199–210, 2019.
- [22] M. Najaf Najafi, R. Kadkhodaei, and S. A. Mortazavi, "Effect of drying process and wall material on the properties of encapsulated cardamom oil," *Food Biophysics*, vol. 6, no. 1, pp. 68–76, 2011.
- [23] Z. Fang and B. Bhandari, "Effect of spray drying and storage on the stability of bayberry polyphenols," *Food Chemistry*, vol. 129, no. 3, pp. 1139–1147, 2011.
- [24] R. V. Tonon, C. Brabet, and M. D. Hubinger, "Anthocyanin stability and antioxidant activity of spray-dried açai (*Euterpe oleracea* Mart.) juice produced with different carrier agents," *Food Research International*, vol. 43, no. 3, pp. 907–914, 2010.
- [25] S. Parrarud and A. Pranee, "Microencapsulation of Zn-Chlorophyll pigment from pandan leaf by spray drying and its characteristic," *International Food Research*, vol. 17, pp. 1031–1042, 2010.
- [26] A. A. Mahalleh, P. Sharayei, and E. Azarpazhooh, "Investigating the characteristics of the *Nepeta binaludensis* encapsulated extract and its release kinetics in laboratory conditions," *Food and Bioprocess Technology*, vol. 14, no. 1, pp. 164–176, 2021.

- [27] P. Montero, M. M. Calvo, M. C. Gómez-Guillén, and J. Gómez-Estaca, "Microcapsules containing astaxanthin from shrimp waste as potential food coloring and functional ingredient: characterization, stability, and bioaccessibility," *LWT-Food Science and Technology*, vol. 70, pp. 229–236, 2016.
- [28] N. M. Sachindra and N. S. Mahendrakar, "Process optimization for extraction of carotenoids from shrimp waste with vegetable oils," *Bioresour Technol*, vol. 96, no. 10, pp. 1195–1200, 2005.
- [29] M. F. Ramadan, L. W. Kroh, and J. T. Mörsel, "Radical scavenging activity of black cumin (*Nigella sativa* L.), coriander (*Coriandrum sativum* L.), and Niger (*Guizotia abyssinica* Cass.) crude seed oils and oil fractions," *Journal of Agricultural and Food Chemistry*, vol. 51, no. 24, pp. 6961–6969, 2003.
- [30] M. Ahmed, M. S. Akter, J. C. Lee, and J. B. Eun, "Encapsulation by spray drying of bioactive components, physicochemical and morphological properties from purple sweet potato," *LWT-Food Science and Technology*, vol. 43, no. 9, pp. 1307–1312, 2010.
- [31] S. Krishnan, R. Bhosale, and R. S. Singhal, "Microencapsulation of cardamom oleoresin: Evaluation of blends of gum Arabic, maltodextrin and a modified starch as wall materials," *Carbohydrate Polymers*, vol. 61, no. 1, pp. 95–102, 2005.
- [32] P. Sharayei, E. Azarpazhooh, and H. S. Ramaswamy, "Effect of microencapsulation on antioxidant and antifungal properties of aqueous extract of pomegranate peel," *Journal of Food Science and Technology*, vol. 57, no. 2, pp. 723–733, 2020.
- [33] S. A. Mahdavi, S. M. Jafari, E. Assadpoor, and D. Dehnad, "Microencapsulation optimization of natural anthocyanins with maltodextrin, gum Arabic and gelatin," *International Journal of Biological Macromolecules*, vol. 85, pp. 379–385, 2016.
- [34] H. Rajabi, M. Ghorbani, S. M. Jafari, A. S. Mahoonak, and G. Rajabzadeh, "Retention of saffron bioactive components by spray drying encapsulation using maltodextrin, gum Arabic and gelatin as wall materials," *Food Hydrocolloids*, vol. 51, pp. 327–337, 2015.
- [35] Q. A. Al-Maqtari, J. K. Mohammed, A. A. Mahdi et al., "Physicochemical properties, microstructure, and storage stability of *Pulicaria jaubertii* extract microencapsulated with different protein biopolymers and gum Arabic as wall materials," *International Journal of Biological Macromolecules*, vol. 187, pp. 939–954, 2021.
- [36] R. Klinjapo and W. Krasaekoopt, "Microencapsulation of color and flavor in confectionery products," in *In natural and artificial flavoring agents and food dyes*, pp. 457–494, Academic press, 2018.
- [37] B. Akdeniz, G. Sumnu, and S. Sahin, "Microencapsulation of phenolic compounds extracted from onion (*Allium cepa*) skin," *Journal of food Processing and Preservation*, vol. 42, no. 7, Article ID e13648, 2018.
- [38] S. A. Mahdavi, S. M. Jafari, M. Ghorbani, and E. Assadpoor, "Spray-drying microencapsulation of anthocyanins by natural biopolymers: a review," *Drying Technology*, vol. 32, no. 5, pp. 509–518, 2014.
- [39] N. N. Condurache, I. Aprodu, O. Crăciunescu et al., "Probing the functionality of bioactives from eggplant peel extracts through extraction and microencapsulation in different polymers and whey protein hydrolysates," *Food and Bioprocess Technology*, vol. 12, no. 8, pp. 1316–1329, 2019.
- [40] Y. Chen, N. He, T. Yang et al., "Fucoxanthin loaded in palm stearin- and cholesterol-based solid lipid nanoparticle-microcapsules, with improved stability and bioavailability in vivo," *Marine Drugs*, vol. 20, no. 4, p. 237, 2022.
- [41] E. Azarpazhooh, P. Sharayei, X. Rui, M. Gharibi-Tehrani, and H. S. Ramaswamy, "Optimization of wall material of freeze-dried high-bioactive microcapsules with yellow onion rejects using simplex centroid mixture design approach based on whey protein isolate, pectin, and sodium caseinate as incorporated variables," *Molecules*, vol. 27, no. 23, p. 8509, 2022.
- [42] M. Harguindeguy and D. Fissore, "On the effects of freeze-drying processes on the nutritional properties of foodstuff: a review," *Drying Technology*, vol. 38, no. 7, pp. 846–868, 2020.
- [43] M. Vakarelova, F. Zanon, G. Dona et al., "Microencapsulation of astaxanthin by ionic gelation: effect of different gelling polymers on the carotenoid load, stability and bioaccessibility," *International Journal of Food Science and Technology*, vol. 58, no. 5, pp. 2489–2497, 2023.
- [44] J. Huang, X. Feng, S. Zhang, L. Wang, J. Yue, and L. Chu, "Preparation and characterization of astaxanthin loaded microcapsules and its application in effervescent tablets," *Journal of the Science of Food and Agriculture*, vol. 103, no. 3, pp. 1421–1431, 2023.
- [45] N. Choudhury, M. Meghwal, and K. Das, "Microencapsulation: an overview on concepts, methods, properties and applications in foods," *Food Frontiers*, vol. 2, no. 4, pp. 426–442, 2021.
- [46] Z. Saavedra-Leos, C. Leyva-Porras, S. B. Araujo-Díaz, A. Toxqui-Terán, and A. J. Borrás-Enríquez, "Technological application of maltodextrins according to the degree of polymerization," *Molecules*, vol. 20, no. 12, pp. 21067–21081, 2015.
- [47] Z. Jia, Y. Xu, J. Wang, and R. Song, "Antioxidant activity and degradation kinetics of astaxanthin extracted from *Penaeus sinensis* (*Solenocera crassicornis*) byproducts under pasteurization treatment," *LWT*, vol. 152, p. 112336, 2021.
- [48] L. Yang, X. Qiao, J. Liu et al., "Preparation, characterization and antioxidant activity of astaxanthin esters with different molecular structures," *Journal of the Science of Food and Agriculture*, vol. 101, no. 6, pp. 2576–2583, 2021.
- [49] X. Zhang, X. Ren, X. Zhao, H. Liu, M. Wang, and Y. Zhu, "Stability, structure, and antioxidant activity of astaxanthin crystal from *Haematococcus pluvialis*," *Journal of the American Oil Chemists' Society*, vol. 99, no. 5, pp. 367–377, 2022.
- [50] C. W. Fong, *The Origin of the Antioxidant Capacity against Oxidative and Photooxidative Stress, Singlet Oxygen Reactivity, and the Excited States in Skin and Eye Related Diseases of Astaxanthin and Other Carotenoids, Isomers and Esters in the Cell Membrane and Cytosol*, Eigenenergy, Adelaide South Australia Australia, 2023.